KEK Preprint 97-131
August 1997
M

A Fast Detector Using Stacked Avalanche Photodiodes for X-ray Diffraction Experiments with Synchrotron Radiation

S. KISHIMOTO, N. ISHIZAWA and T. P. VAALSTA

Submitted to Review of Scientific Instruments.

** From April 1, 1997, **High Energy Accelerator Research Organization (KEK)** was newly established. The new organization is restructured of three reseach institutes, National Laboratory for High Energy Physics (KEK), Institues of Nuclear Study (INS), Univ. of Tokyo and Meson Science Laboratory, Faculty of Science, Univ. of Tokyo.*

High Energy Accelerator Research Organization (KEK), 1997

KEK Reports are available from:

Information Resources Division
High Energy Accelerator Research Organization (KEK)
1-1 Oho, Tsukuba-shi
Ibaraki-ken, 305
JAPAN

Phone: 0298-64-5137
Fax: 0298-64-4604
Cable: KEK OHO
E-mail: Library@kekvax.kek.jp (Internet Address)
Internet: http://www.kek.jp

A fast detector using stacked avalanche photodiodes for X-ray diffraction experiments with synchrotron radiation

S. Kishimoto[a], N. Ishizawa[b] and T. P. Vaalsta[c]

[a]Photon Factory, Institute of Materials Structure Science, 1-1 Oho, Tsukuba, Ibaraki 305, Japan

[b]Materials and Structures Laboratory, Tokyo Institute of Technology, Nagatsuta, Midori, Yokohama 226, Japan

[c]Crystallography Centre, University of Western Australia, Nedlands, Perth WA 6907, Australia

Abstract

We have developed a fast detector using stacked avalanche photodiodes for X-ray diffraction experiments with synchrotron radiation. This detector has four independent channels of APDs, and the detector efficiency has reached 55% in all for 16.53-keV X-rays. Since the dead time of the counting system is shorter than 4 ns, output rates of up to 4.5×10^8 counts/s have been obtained for 16.53-keV X-rays. The dynamic range is more than 10^{10} in the multi-bunch mode of a storage ring. Pulse-height measurements at output rates of up to 10^8 counts/s were successfully carried out by sequential single-channel discrimination.

Key words: X-ray detector, avalanche photodiode, fast counting, synchrotron radiation, X-ray diffraction

I. INTRODUCTION

In X-ray diffraction experiments using synchrotron radiation, such as charge density studies, a wide dynamic range is needed for the output rate of the detector. If the detector has a wide dynamic range of its output rate, we can obtain a better accuracy for the structure factors determined by the integrated intensities of the reflection spots.[1] When the pulse-counting method is used for the measurements, the lower limit of the dynamic range is determined by the background noise, and the upper limit is given by the dead time of the counting system. The dead time of a conventional detector is longer than several microseconds. For example, the outputs from a NaI(Tl) scintillation detector saturate at rates of over 10^5 counts/s. Therefore, a counting system does not easily have a dynamic range of more than 10^7. On the other hand, an X-ray detector using an avalanche photodiode (APD) has a short dead time of a few nanoseconds. This enables an observed rate of more than 10^8 counts/s in the multi-bunch mode of a storage ring.[2] Since the noise level of the APD detector is less than 10^{-2} counts/s, we can obtain a dynamic range of more than 10^{10}.

However, the sensitive thickness of APDs has been limited to be about 100 μm due to a technical difficulty in the fabrication. This leads to a low efficiency for X-rays of energies higher than 10 keV; the efficiency is 23% for 100 μm of silicon at 14.4keV. A simple and good idea for increasing the efficiency by a factor of two or more is to incline the device to the incident beam.[3] This method can be applicable to experiments using a small-area beam and a large-area device. Note that the maximum rate of the detector outputs decreases with increasing area of the device. This is because the pulse width from an APD becomes long when the electric capacity of the device increases with the effective area. If some devices having relatively small areas are stacked, no deficit of the count-rate capability occurs. The total efficiency increases to the sum of that for each diode. Moreover, when using a stack of devices, the load of the output rate per device decreases at a high energy of X-rays, where the partial absorption is nearly equal among the devices. When we use the existing devices for the stacked detector, however, they still have some problems in the

structure. One device has a thick dead region, such as a surface dead-layer of 40-50 μm of silicon[4] and a wafer, itself, of silicon several hundreds μm. A layer of metal, such as gold, of several thousands Å sometimes exists at the backside of an APD device as an electrode. Then, the incident beam may almost be absorbed at the dead regions of the front device, and thus may not reach other devices in the stack. In addition, if the incident beam has an energy higher than those of the L-absorption edges of gold (11.92, 13.73 and 14.35 keV), the gold backing causes fluorescence X-rays, which may disturb the measurement of the incident beam. Therefore, the thickness of the dead region should be reduced as much as possible, and no metallic backing is needed for stacked devices.

There have been some reports concerning stacked or multi-layer semiconductor detectors.[5,6] However, the stacking arrangement of APDs has never succeeded in an application. No APD has had a structure suitable for beam transmission. A new APD device suitable for mounting in a stack has recently been developed, and we have investigated performance of a fast detector using a stack of the APDs. Here, we describe the results obtained with the APD detector and a fast counting system. The APD detector has been applied to X-ray diffraction experiments using a four-circle diffractometer installed at beamline BL14A of the Photon Factory (PF). The wide dynamic range of the APD detector successfully improved the accuracy for experiments on the charge density. The result is presented in another paper.[7]

II. Detector and counting system

The detector consists of a stack of four silicon avalanche photodiodes, perpendicular to the incident beam. Each device is an SPL2625 (No.1-4, Hamamatsu Photonics) having a detection area of 2.8 mm in diameter. This device has a reach-through structure[8] and a depletion region of more than 100 μm. On the opposite side of an n+-p junction, a wafer was etched from the surface, and only a thin dead layer of p+ remains there.[9] The surface of n+ is covered by a thin layer of SiO_2,

without a gold electrode inside of the sensitive area. The tip of APD is mounted on an epoxy plate having a hole (3 mm in diameter), by putting the n+ side up. Thus, other devices placed behind can detect the X-ray beam while thin dead layers may exist on both surfaces of the front device. The arrangement of stacked APDs is shown schematically in Fig.1. In the present detector, the X-ray beam comes from the n+ side of the APD. This setup was adopted only due to the point of easier detector fabrication. The distance between the APDs is 2 mm. A negative voltage is applied to all diodes in common from the p+ electrode. Negative signals from each APD are taken from the n+ electrode independently.

Four fast amplifiers (Phillips Scientific 6954) are used for amplifying the signal from each APD. The amplifier's gain is 100. The APD devices are contained in a small stainless-steel chamber with a beryllium window (130 μm thick). The small chamber and the amplifiers are fixed together on an aluminum plate. The signals from the amplifiers are sent to a CAMAC system, which has discriminators (Technoland C-TM415) and a counter (Technoland C-KP402). Each channel of the discriminator can be set by 10-bit resolution of the threshold for the -1 V range. If a pulse splitter before the discriminator divides each signal into two pulses, the number of counts with a lower threshold level (LL) and that with an upper level (UL) can be recorded at the same time using the system. Then, the number of counts in the window width is obtained by subtracting the number of counts with UL from that with LL. A counting system equipped with such pulse-height discrimination is illustrated in Fig. 2. The discriminator gives a response of the non-updating mode, or having a fixed dead time. The pulse-pair resolution of the discriminators is 3.3 ns. The maximum counting rate of the counter is 300 MHz. Setting the threshold levels of the discriminators and reading data in each channel of the counter are controlled by a personal computer. This system has been opened for users at BL14A since April 1996.

III. Detector properties

A. Experimental setup

We investigated the performance of the APD detector and the counting system. The measurements were carried out at vertical wiggler beamline BL14A of PF.[10] A double-crystal silicon (111) monochromator was used to define an X-ray energy to 8.05 keV or to 16.53 keV. A bent cylindrical mirror focused a monochromatic beam and removed the harmonics. The APD detector was mounted on the 2θ arm of a four-circle diffractometer installed at BL14A. The setup is schematically shown in Fig. 3. The X-ray beam was defined by slits up to 1×1 mm. The beam intensity through the slits was monitored all the time by an ionization chamber located behind the slits. The intensity onto the APD detector was varied by changing the thickness or the number of metal foils, as attenuators, inserted just in front of the detector. Copper foils were used for measurement at 8.05 keV and molybdenum foils were used for that at 16.53 keV. The transmission rates of the foils were measured one by one. The pulse splitter shown in Fig. 2 was not used for the performance test.

B. APD's gain and output signals

An example of the variation of the APD's gain against the applied voltage (negative) is shown in Fig. 4. The squares represent the data of an APD (SPL2625, No. 5), observed with 16.53-keV X-rays at room temperature (21°C). The values of the gain (M) were calibrated using the mean energy (w), producing an electron-hole pair in silicon (3.63 eV at 300 K[11]) and the charge quantity (Q) measured with a charge-sensitive preamplifier (CANBERRA 2001A) and with a pulser (ORTEC 448). The peak position on the energy spectrum for the APD was recorded at an applied voltage with a spectroscopy amplifier (ORTEC 572) and a multi-channel analyzer system (CANBERRA 8077 and FAST ComTec MCD/PC). The input voltage of the preamplifier (V (V)) from the APD was determined by adjusting the output voltage of the pulser to the peak position on the energy spectrum through the test input that had a charge sensitivity of 0.5 pC /V. At the X-ray energy (E

(eV)), M is given by Q/q, where $q = 1.60 \times 10^{-19} \times E / w$ (C) and $Q = 0.5 \times V \times 10^{-12}$ (C). At a voltage lower than 95 V, the dark current of the APD disturbed the observation of the peak profile on the energy spectrum. The energy resolution became much worse at voltages beyond 700 V, and the gain increased rapidly at a voltage higher than 750 V. Therefore, we used the detector at a bias voltage lower than 700 V and at a gain of about 50. The deviation of the gain among the diodes (No. 1-4), mounted in the detector, was within ±10% at 700 V.

Figure 5 (a) shows the outputs from the fast amplifier of Channel 1, for 8.05 keV and 16.53 keV. The applied voltage was -700 V and the gain was 50 in this case. The leading edge of the pulse roughly had the same time of 1.0 ns as the tail. The half width was 1.7 ns, and the width on the base line was 3.2 ns. The discriminator output is shown in Fig. 5 (b). This is a NIM-standard fast negative pulse. The output width was set to a minimum, and was 1.7 ns at the half and 3.9 ns at the bottom.

C. Thickness of the sensitive region and dead layers

The thickness of the sensitive region and dead layers was estimated from the experiments using another chamber with one APD plate (SPL2625, No. 6). The structure of the device is assumed in Fig. 6 (a); the thickness of the surface dead layer on the p+ side is t_{x1}, that of the sensitive region is t_{x2}, and that of the surface dead layer on the n+ side is t_{x3}. Figure 6 (b) shows a schematic setup of the experiment. X-rays of 8.05-keV were used and a beam of less than 1 × 1mm was irradiated at the center of the detection area of the device. After (A) measuring the beam intensity with a NaI(Tl) scintillation detector (OKEN SP-10), both (B) the number of counts with the single APD and (C) that measured with the NaI behind the chamber were simultaneously recorded for a mount in which the n+ was the front side. Next, the chamber was rotated through 180° so that the front side was changed to p+. Then, the same measurement was carried out. The counts of (D) were then measured with the APD and (E) was recorded with NaI. The test chamber had two beryllium

windows of 130 μm on both sides. The thickness of air was 14 mm from the window to the n+ surface, and was 6 mm from the window on the opposite side to the p+ surface. For measurements under a better energy resolution, the APD was operated at a low gain of about 25 while measuring the energy spectrum with the spectroscopy system described in Section III.B. It was confirmed that the thickness of depleted region was the same as at the gain of 50 from a measurement of the electric capacity of the device. While measuring the NaI detector, a delay-line amplifier (ORTEC 460) and a single-channel analyzer (ORTEC 551) were used. Here, the absorption at the first beryllium window was neglected, because the thickness of the window was the same as that of the NaI detector. The input photon rate was 3.5×10^3 photons/s. A slight change of the beam intensity was also corrected using the average current of the ionization chamber.

The value of t_{x1} is expressed by the observed counts of A, B and C:

$$t_{x1} = \frac{-\ln\left(\frac{C}{A\exp(-\mu t_{x3}) - B}\right)}{\mu}. \qquad (1)$$

Here, the dead layers are assumed to all be silicon, and μ is the linear-absorption coefficient for silicon at 8.05 keV, given by 144 cm^{-1}.[12] The value of t_{x3} is also expressed with the counts of A, D and E:

$$t_{x3} = \frac{-\ln\left(\frac{E}{A\exp(-\mu t_{x1}) - D}\right)}{\mu}. \qquad (2)$$

The values of t_{x1} and t_{x3} were obtained from eqs. (1) and (2) using the counts of (A)-(E), which were corrected for absorption in air and in the beryllium window. Thus, the values of t_{x1} and t_{x3} were given by 0.7±0.5 and 2.5±0.5 μm, respectively. The whole thickness of the device was given by

$$t_{x1} + t_{x2} + t_{x3} = \frac{-\ln\left(\frac{C}{A}\right)}{\mu} = \frac{-\ln\left(\frac{E}{A}\right)}{\mu}. \qquad (3)$$

According to this equation, the whole thickness was 135±1 μm. Then, the value of t_{x2} was given by 132±1 μm. For obtaining the maximum efficiency with this APD, it is better to make the p+ side up to the incident beam, since the dead layer of the p+ surface is thinner than that of the n+ side.

The thickness of the sensitive region was also measured with 16.53-keV X-rays. By dividing (B') the number of counts with the APD by (A') that with the NaI detector, the absorption at the sensitive region was obtained to be similar to that at 8.05 keV. In this measurement, the absorption at the dead layers of silicon less than 5 μm and in air of 14 mm was neglected, since the X-ray energy was high. Thus, the thickness of the sensitive region was given by 118 ± 1 μm. Even if the absorption at the dead layer on the surface and in air was considered, the difference was within the error. The smaller thickness of the sensitive region may have been due to the longer path length of photoelectrons in silicon, which are ejected during ionization by X-rays.

D. Counting behavior and efficiency

We investigated the counting behavior of the detector system with a direct beam of synchrotron X-rays. When measuring counts with synchrotron radiation, we had to consider the pulsed nature of the beam in order to evaluate the count loss and linearity, because synchrotron radiation has a time structure that is attributed to bunches of charged particles (electrons or positrons) in the orbit of a storage ring. The bunch interval is a few microseconds in the single-bunch mode, or a few nanoseconds in the multi-bunch mode. Then, the dead time of the counting system, depending on the electronics, determines the behavior by being compared with the time interval of the pulsed beams. Moreover, if some photons arrive at a detector within one bunch, of which the width is

several hundreds of picoseconds, it is important what number of events the detector can count per bunch period through its efficiency. The maximum number is normally limited to be one event. Finally, the behavior of the system depends on the bunch interval, efficiency of the detector and pulse processing in the electronics.

Here, we present models for a detector operated in the multi-bunch mode of a storage ring.[13] A time structure of bunches is given for the multi-bunch mode of the PF ring, as shown in Fig. 7. There are 280 electron bunches and an empty region of 32 buckets in the orbit. This mode was selected for maintaining a stable operation with electron injection. The accelerating radio frequency (f) was 500.2 MHz and the bunch interval ($1/f$) was 2.0 ns. Thus, the number of bunches observed in unit time is expressed by $f'(=f\times(280/312))$. We consider that the detector has four independent channels for counting. The channels have different values of efficiency due to different locations in the stack. When the observed rate is expressed by m (counts/s), the behavior is given for a system having an extended dead time by the model:

$$m=\sum_{i=1}^{4} f'\left(1-\exp\left(-\frac{\varepsilon_i n}{f'}\right)\right)\exp\left(-\frac{(k-1)\varepsilon_i n}{f'}\right). \tag{4}$$

For a system having a non-extended dead time, the behavior is given by the model:

$$m=\sum_{i=1}^{4}\frac{f'\left(1-\exp\left(-\frac{\varepsilon_i n}{f'}\right)\right)}{1+(k-1)\left(1-\exp\left(-\frac{\varepsilon_i n}{f'}\right)\right)}. \tag{5}$$

Here, ε_i (i=1-4) is the intrinsic efficiency of each APD, and n is the input photon rate (photons/s). The dead time of the counting system (τ) satisfies the relation that $(k\text{-}1)/f<\tau<k/f$, where k is an integer (1,2,...).

Variation in the output count rate (OCR) as a function of the input photon rate (IPR) was observed at 8.05 and 16.53 keV. The output rate was obtained from counts measured for 100 s with the APD detector. The threshold level was set to -10 mV. Then, the background counts were zero for 100 s. The input rate was obtained from the counts measured with the NaI detector, just after a measurement with the APD detector and from transmission rates for foils additionally inserted for the NaI measurement. The output rates of the NaI were less than 4.0×10^3 counts/s with adjusting the thickness of the metal foils. The component of the harmonics in the beam was carefully checked by measuring the energy spectrum, and was less than 2% of the fundamental. Therefore, the effects of the pulse pile-up and of the harmonics were neglected. The background counts of the NaI were measured without the incident beam. Except for the absorption of X-rays at the beryllium window, the intrinsic efficiency of the NaI detector could be estimated to be unity because the crystal was 1.5 mm thick, enough for 16.53 keV; also, it had no absorbers between the beryllium window and the crystal. The window thickness of the NaI detector was the same as that of the APD detector. Thus, the efficiency of the APD detector was defined by dividing the observed counts with the APD detector by those measured with the NaI detector, without the absorption at the beryllium window.

Figure 8 (a) shows the variation in the OCR observed at 8.05 keV. The results measured at 16.53 keV are shown in Fig. 8 (b). The closed circles are plotted as the sum of the rates for the four channels, and the open circles are plotted as the rates for Channel 1. The error for the rates, estimated from the Poisson statistics, was less than 0.7% for the IPR, which was larger than that for the OCR. The error bar is within the diameter of the plotted circles. The calculated curves on the models of eq. (4) and of eq. (5) are also plotted for both Channel 1 and the sum of Channels 1-4. Here, k=2 was taken for the calculation, since both the output width of the amplifier and the pulse-pair resolution of the discriminator were shorter than 4 ns. The solid curves were given by the model of eq. (4) and the dashed curves were given by that of eq. (5). The values of the intrinsic

efficiency were determined from a linear fitting of 4 data at lower input rates. They were used for ε_i in eq. (4) and eq. (5). The values of ε_i are listed in Table 1. Here, the device of Channel 1 was located on the incident side. By stacking four APD plates, we could obtain a value of the detector efficiency (54.9%), about three-times larger than that for one plate at 16.53 keV. The upper limit of the OCR was more than 10^8 counts/s at both energies. At 8.05 keV, the total output rates gradually increased to 2.99×10^8 counts/s at the input rate of 4.44×10^9 photons/s, as seen in Fig. 8 (a). At 16.53 keV in Fig. 8 (b), the output rate reached a maximum of 4.57×10^8 counts/s at 7.96×10^9 photons/s, and slightly decreased to 4.53×10^8 counts/s at 1.34×10^{10} photons/s. Thus, the dynamic range of the APD detector was more than 10^{10}, because the noise rate was less than 10^{-2} counts/s.

Figure 9 shows the variation in the ratio of the OCR of Channel 1 to the rate calculated (CAL) by each model. There are no evident differences between the two models in the range of IPR, lower than 2×10^7 photons/s at 8.05 keV, as shown in Fig. 9 (a), and lower than 1×10^8 photons/s at 16.53 keV, as shown in Fig. 9 (b). However, the deviation from the calculated values becomes larger with increasing input rate. Maximum values of 4% and 10% are seen in the results at 8.05 keV and 16.53 keV, respectively. This slope may indicate a systematic error caused by the transmission rates of the metal foils, which were smaller than the true values. If the slope is corrected, the deviation is less than 1% at 8.05 keV and less than 2.5% at 16.53 keV. At input rates of 5×10^7 and 4×10^8 photons/s for 8.05-keV, the observed output rates correspond to the model of eq. (4) rather than that of eq. (5). Also for 16.53 keV, the model of eq. (4) gives a better fit for the data observed at 4×10^8 and 1.5×10^9 photons/s. The model of the extended dead time, written in eq. (4), shows that the output rate of each channel has a maximum of $m_{max} (=f'/k \times (k-1/k)^{k-1})$ at an input rate of $n_{max} (=f'/\varepsilon_i \times \ln(k/k-1))$. For the present cases, m_{max} for Channel 1 is given by 1.12×10^8 counts/s at 3.76×10^8 photons/s for 8.05 keV and at 1.67×10^9 photons/s for 16.53 keV. When the systematic error mentioned above is corrected, the observed behavior corresponds within a

difference of 10% to the values calculated by the model of eq. (4). As described in the reference,[13] the response of the counting system depends on the k value. In more detail, k_A and k_P are defined as the value determined by the amplifier's outputs and that by the response of a discriminator and a scaler, respectively. The behavior of a system having $k_A = k_P$ is expressed by the model of extended dead time, even if the discriminator has a non-extended dead time. The above result is reasonable, since the present system has $k_A = k_P = 2$. However, beyond the IPR where the OCR of each device reached the maximum, a rapid decrease of the OCR did not occur, which the extended dead-time model predicted; it seems that the OCR experienced the saturation different from the non-extended dead-time model. At such high rates, the discriminator might not have an ideal response because the input signals overlap each other, and their shape is greatly changed from a single pulse.

Figure 10 shows the count loss ($\varepsilon \times$ICR-OCR)/ $\varepsilon \times$ICR) at both energies. Here, the OCR is the sum of Channel 1-4, and ε is the total efficiency. After correcting the slope due to a systematic error, a count loss of 20% occurs at 1×10^8 photons/s of 8.05 keV, while it is about 5% at 16.53 keV. This is based on the fact that the mean number of events recorded in the detector per bunch, which depends on the efficiency, approaches unity. Then, the count loss often occurs due to successive pulses since the dead time is longer than the bunch interval (2 ns). From a calculation using the model of eq. (4), the range of linearity, where the count loss is less than 5%, is limited to up to 1.54×10^7 photons/s for a system having an efficiency of $\varepsilon = 1$ and a dead time shorter than 4 ns ($k = 2$). Nevertheless, it is noted that the upper limit of the range, linear within 5% to the response of the model, is more than 10^8 counts/s in the present system, even at 8.05 keV, as shown in Fig. 9 (a).

E. Pulse-height distribution

Figure 11 (a) shows an energy spectrum for one of the SPL2625 (No. 5) mounted in the test chamber. It was measured with the same spectroscopy system as described in Section III. B. A full

width of half maximum (FWHM) of 21% was obtained at 16.53 keV. The gain was about 50. Another measurement was performed for obtaining the pulse-height distribution with the fast counting system shown in Fig. 2. Figure 11 (b) shows a plot by sequential single-channel discrimination. This method is based on serially recording counts passed by the same discriminator having a threshold. The threshold level is repeatedly scanned to cover the range of the pulse height. We thus obtain the number of counts within the width of the pulse height by subtracting the number of counts at the upper level from that at the lower level. The window width was a minimum, one in 10 bits, which was 1.3 mV in the threshold level. Thus, the distribution in Fig. 11 (b) is almost the same as that in (a). Here, in figure (b), the peak of the pulse height is 1.4-times as high as the peak of the threshold level. This is because the discriminator processes a pulse that has a width longer than 1.4 ns at its threshold level.

Although the distribution in Fig. 11 (b) was measured at a moderate count rate of 6×10^4 counts/s, this method has the advantage of availability at high output rates, such as more than 10^6 counts/s, where multi-channel analyzer systems do not work. Figures 12 (a) – (d) show plots of pulse-height distribution of the APD detector (Channel 1), recorded at various OCR / IPR for 8.05-keV X-rays using this method. Even at a rate of 2.2×10^7 photons/s, the pulse-height distribution was not much deformed, shown in Fig. 12 (b). The second and the third peaks become clear in (c) at 2.3×10^8 photons/s and more in (d) at 5.7×10^8 photons/s. Although the peak positions are changed due to a baseline shift of the amplifier's DC level and tail pile-up of the input pulses, these peaks correspond to the events of the multiple photons per bunch. The probability of observing x events per bunch with Channel i of the detector is given by

$$P(x) = \frac{(\frac{\varepsilon_i n}{f'})^x \exp(-\frac{\varepsilon_i n}{f'})}{x!} . \qquad (6)$$

Here, $P(x)$ is expressed by assuming that the number of x follows a Poisson distribution. The symbols of ε_i, n and f' are the same as defined in eqs. (4) and (5). According to eq. (6), the probabilities for single-photon events (x=1), two-photon events (x=2) and three-photon events (x=3) are given for Channel 1 of the APD detector (ε_i=0.827) by 0.367, 0.192 and 0.067 at n=5.7×10^8 photons/s, respectively. Table 2 lists these numbers. The probabilities for multiple photon events, normalized to that for single-photon events, are also given in Table 2. They are roughly the same as the ratios of the peak height in (d) for the second peak at 44 mV and the third peak at 66 mV, relative to the height of the first one at 22 mV. Although the resolution became worse, and eventually lost after the OCR reached the maximum, the distribution for single- and multiple-photon events was correctly recorded by this counting system up to 10^8 counts/s.

IV. CONCLUSION

A fast counting system with a detector using stacked avalanche photodiodes was developed for X-ray diffraction experiments. The performance of the APD detector system was investigated with 8.05- and 16.53-keV X-rays of synchrotron radiation. Four diodes were stacked in the detector. The total of the sensitive thickness was estimated to be about 480 μm of silicon and the detection efficiency was 55% at 16.53 keV. This was three-times larger than that for a single diode. The present APD is suitable for mounting in a stack, because it does not have a gold backing or any thick dead layers of silicon. The behavior of the counting system could be explained by the model for synchrotron radiation, up to more than 10^8 counts/s per device, although the discriminator affected the response over the input rate where the maximum of output rate was predicted by the model. The output rate for the sum of 4 channels reached 2.99×10^8 counts/s at 8.05 keV and 4.57×10^8 counts/s at 16.53 keV. The observation of such high rates is due to a dead time of shorter than 4 ns. On the other hand, the lower limit was less than 10^{-2} counts/s. Therefore, a dynamic range of more than 10^{10} was accomplished by this APD detector. Sequential single-channel discrimination

was applied to a measurement of the pulse-height distribution at high count rates. This method enabled us to record the pulse-height distribution even at 10^8 counts/s. The APD detector distinguished single-photon events from multiple-photon events until the output rate of each device reached the maximum, while the resolution became worse.

We are now preparing another detector that has more than 4 APD channels and an improved system that has a high resolution for pulse-height discrimination. These may expand the use of the APD detector to fields that require high efficiency for X-ray energies higher than 10 keV, a wide dynamic range of the count rate and also a moderate energy resolution, even at rates of up to 10^8 counts/s, simultaneously.

ACKNOWLEDGEMENTS

The authors wish to thank Y. Ishikawa and T. Inuzuka (Hamamatsu Photonics K. K.) for the supply of the APD devices and for useful discussions.

References

[1]P. Coppens, D. Cox, E. Vlieg and I. K. Robinson, Synchrotron Radiation Crystallography, (Academic Press, New York, 1992) p.81.

[2]S. Kishimoto, Rev. Sci. Instrum. 66, 2314(1995).

[3] A. Q. R. Baron and S. L. Ruby, Nucl. Instr. Meth. A343, 517 (1994).

[4]R. Farrell, F. Olschner, E. Fredrick, L. McConchie, K. Vanderpuye, M. R. Squillante and G. Entine, Nucl. Instr. Meth. A288, 137 (1990).

[5]M. Hirata, T. Cho, J. Kohagura, K. Yatsu, T. Tamano, S. Miyoshi, T. Kondoh, Y. Saitoh, K. Sato, S. Miyahara, K. Hirano and H. Maezawa, Rev. Sci. Instrum. 66, 2311 (1995).

[6]EG&G ORTEC Catalog, p. 406 (1995).

[7]S. Kishimoto, N. Ishizawa and T. P. Vaalsta, KEK Proceedings 97-8, p. 254 (1997) and J. Appl. Crystallograpy (to be published).

[8]P. P. Webb, R. J. McItyre, and J. Conradi, RCA Rev., 35, 234(1974).

[9]Y. Ishikawa (Hamamatsu Photonics K. K.), private communication.

[10]Y. Satow and Y. Iitaka, Rev. Sci. Instrum. 60, 2390 (1989).

[11]R. D. Ryan, IEEE Trans. Nucl. Sci. NS-20, 473 (1973).

[12]S. Sasaki, KEK Report 90-16, p. 12 (1990).

[13]S. Kishimoto, Nucl. Instr. and Meth. A, in press.

Table 1

Intrinsic efficiency (ε_i) determined by a ratio of the output rate with the APD detector to the input photon rate. Here, the efficiency is defined without the absorption at the beryllium window. The error of each channel was given by ± 0.002.

Channel	ε_i	
	8.05 keV	16.53 keV
1	0.827	0.186
2	0.118	0.149
3	0.016	0.121
4	0.002	0.093
Sum	0.963	0.549

Table 2

Probabilities for single- and multiple-photon events observed per bunch at 5.7×10^8 photons/s of 8.05-keV X-rays with Channel 1 of the APD detector (ε_1 =0.827).

Events	P(x)	P(x), Relative to the single-photon events	Peak ratio, Obtained in Fig. 12 (d)
Single-photon (x=1)	0.367	1	1
Two-photon (x=2)	0.192	0.523	0.51
Three-photon (x=3)	0.067	0.183	0.18

Figure captions

Fig. 1

Schematic draw of the arrangement of stacked avalanche photodiodes (Hamamatsu SPL2625, No. 1-4).

Fig. 2

Fast counting system with the APD detector.

Fig. 3

Schematic of the test setup for the APD detector.

Fig. 4

Variation in the gain as a function of the applied voltage (negative) for SPL2625 (No. 5).

Fig. 5

Observed signals of (a) amplifier outputs of Channel 1, at 8.05 keV and at 16.53 keV, and of (b) discriminator output.

Fig. 6

Estimation of thickness of the sensitive region and the dead layers: (a) the assumed structure of the SPL 2625 and (b) the experimental setup. In (a), the thickness of the dead layer on the p+ surface is given by t_{x1}, that of the sensitive region is t_{x2}, and that of the dead layer on the n+ side is t_{x3}.

Fig. 7

Time structure of electron bunches in the multi-bunch mode of the Photon Factory ring.

Fig. 8

Behavior of the output count rate (OCR) as a function of the input photon rate (IPR) for (a) 8.05 keV and (b) 16.53 keV. The closed circles show the output rates for the sum of Channel 1-4 and the open circles are for the output rates of Channel 1. The solid curves are plotted by eq. (4) and the dashed curves are given by eq. (5).

Fig. 9

Ratio of the output count rate (OCR) to the rate (CAL) calculated by the model of eq. (4) (•) and by the model of eq. (5) (o) for (a) 8.05 keV and (b) 16.53 keV. The values are plotted against the input photon rate (IPR).

Fig. 10

Count loss of (ε×IPR-OCR)/(ε×IPR) as a function of the input photon rate (IPR) for 8.05keV (o) and 16.53 keV (•). Here, ε is the total efficiency and OCR is the output count rate, given by the sum of Channel 1-4.

Fig. 11

Energy spectra of the APD (SPL2625 No. 5, M~50) measured at 16.53 keV: (a) with a charge-sensitive preamplifier and a multi-channel analyzer system and (b) with the fast counting system and sequential single-channel discrimination. The energy resolution was 21% (FWHM). It is noted that the noise level in (b) was higher than 10 mV because the chamber used was different from that at the count-rate measurement.

Fig. 12

Pulse-height distribution of 8.05-keV X-rays with the APD detector (Channel 1) and with sequential single-channel discrimination. Each spectrum was measured at the input / output rate (IPR (photons/s) / OCR (counts/s)): (a) 2.6×10^5 / 2.2×10^5, (b) 2.2×10^7 / 1.8×10^7, (c) 2.3×10^8 / 9.5×10^7 and (d) 5.7×10^8 / 1.0×10^8.

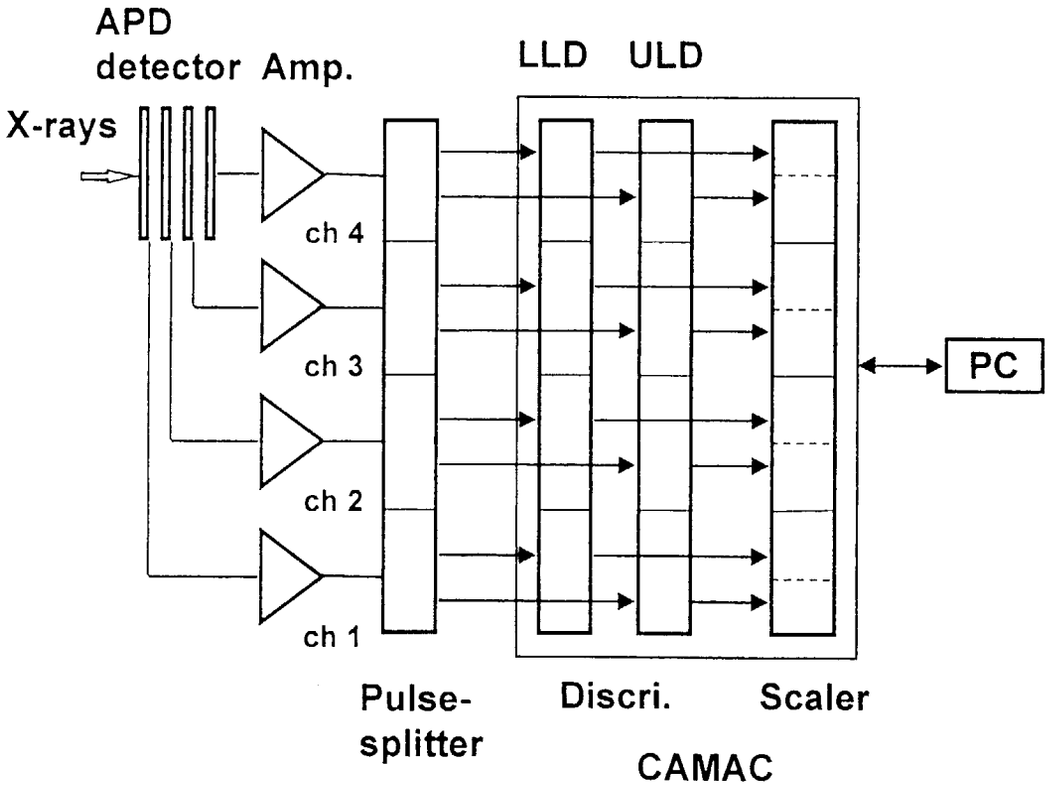
APD
detector
Amp.
LLD
ULD
X-rays
ch 4
ch 3
ch 2
ch 1
PC
Pulse-
splitter
Discri.
Scaler
CAMAC

Fig. 2

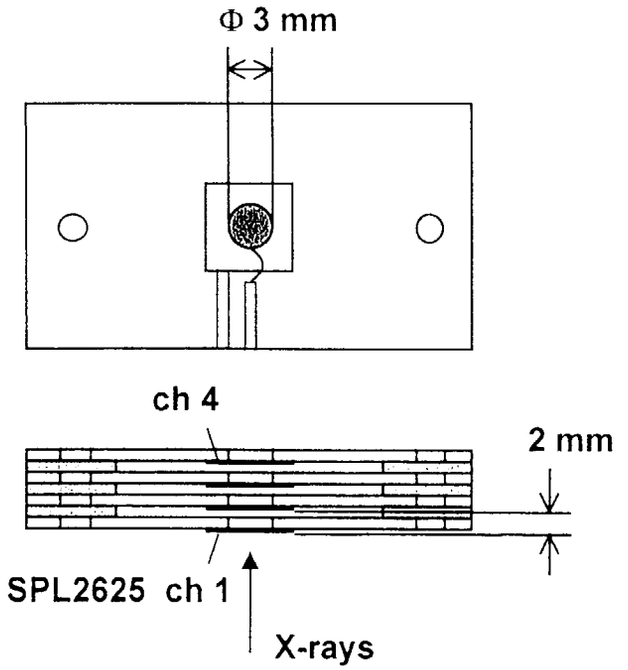
Φ 3 mm
ch 4
2 mm
SPL2625
ch 1
X-rays

Fig. 1

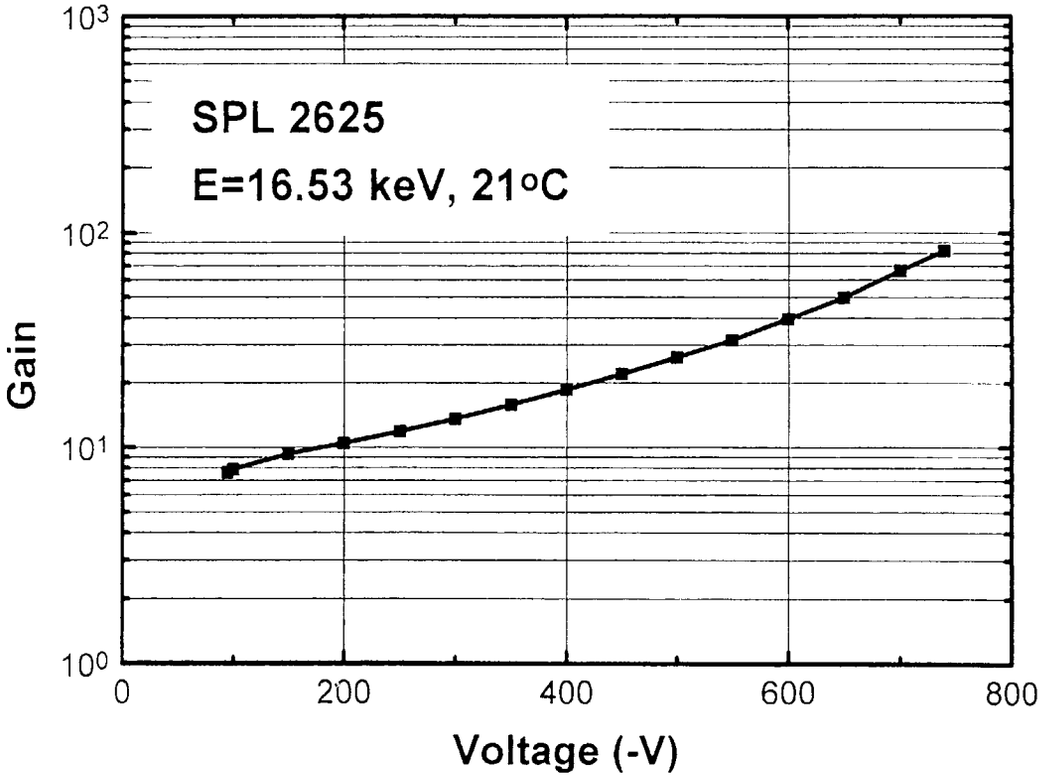
SPL 2625
E=16.53 keV, 21°C
Gain
Voltage (-V)
10^3
10^2
10^1
10^0
0
200
400
600
800

Fig. 4

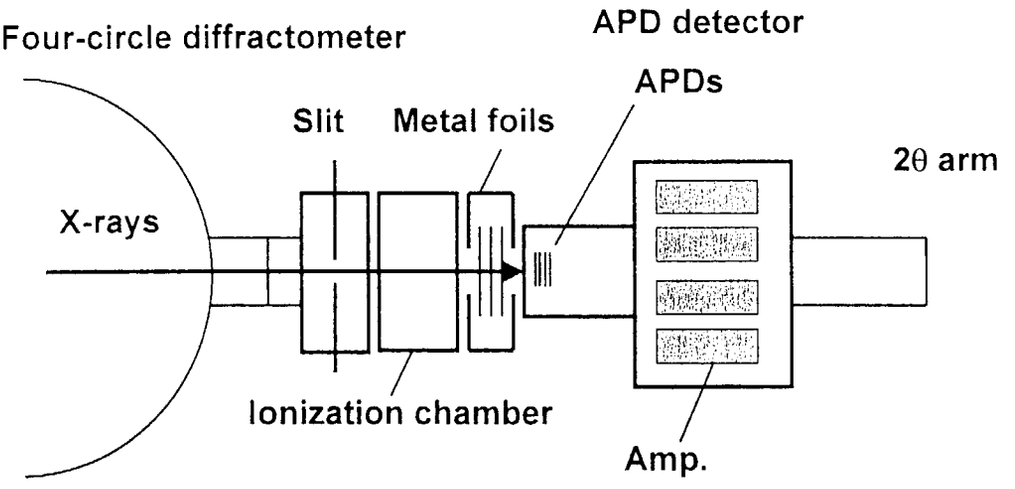
Four-circle diffractometer
APD detector
APDs
Slit
Metal foils
2θ arm
X-rays
Ionization chamber
Amp.

Fig. 3

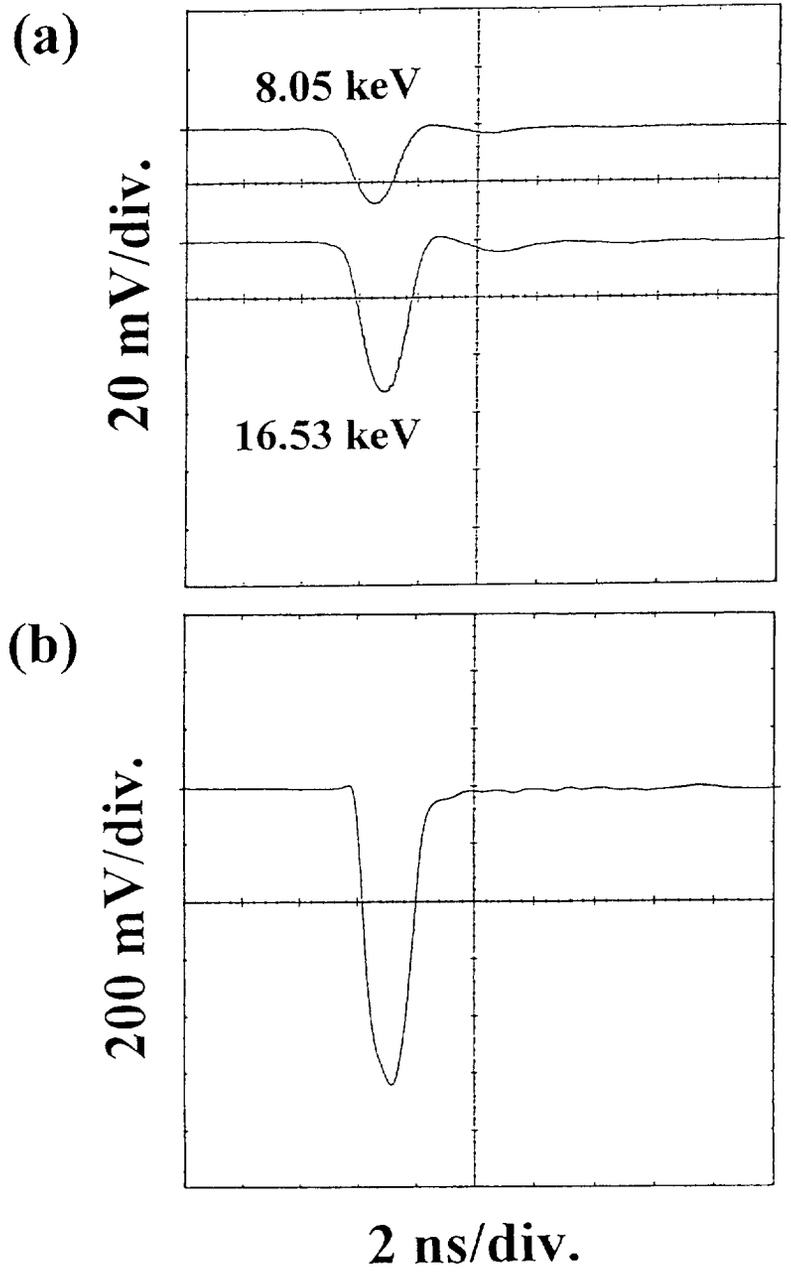
(a)
8.05 keV
16.53 keV
20 mV/div.
(b)
200 mV/div.
2 ns/div.

Fig. 5

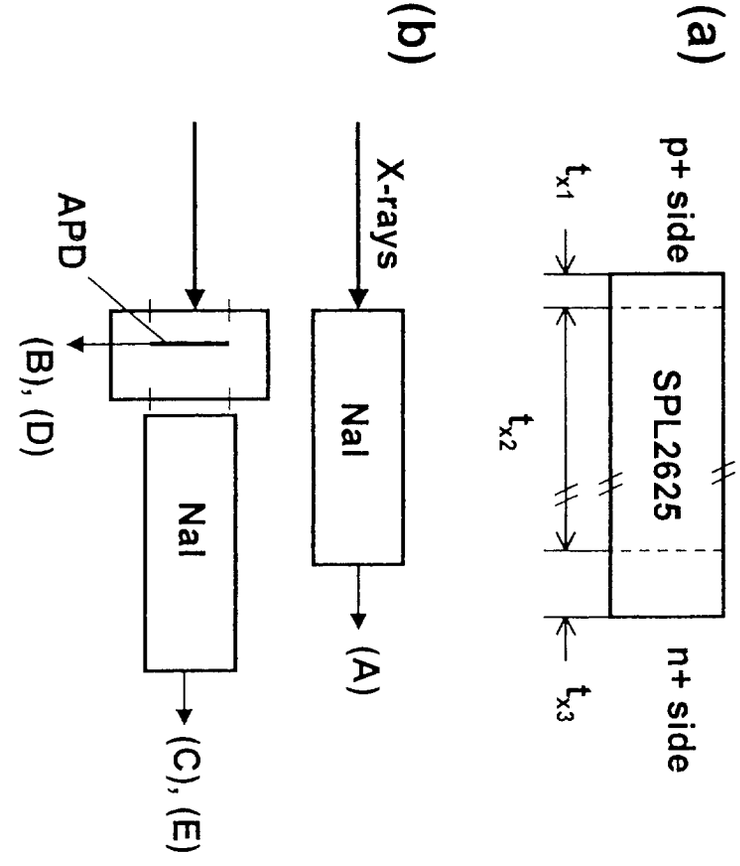
(a)
p+ side
t_{x1}
t_{x2}
SPL2625
t_{x3}
n+ side
(b)
X-rays
NaI
(A)
APD
(B), (D)
NaI
(C), (E)

Fig. 6

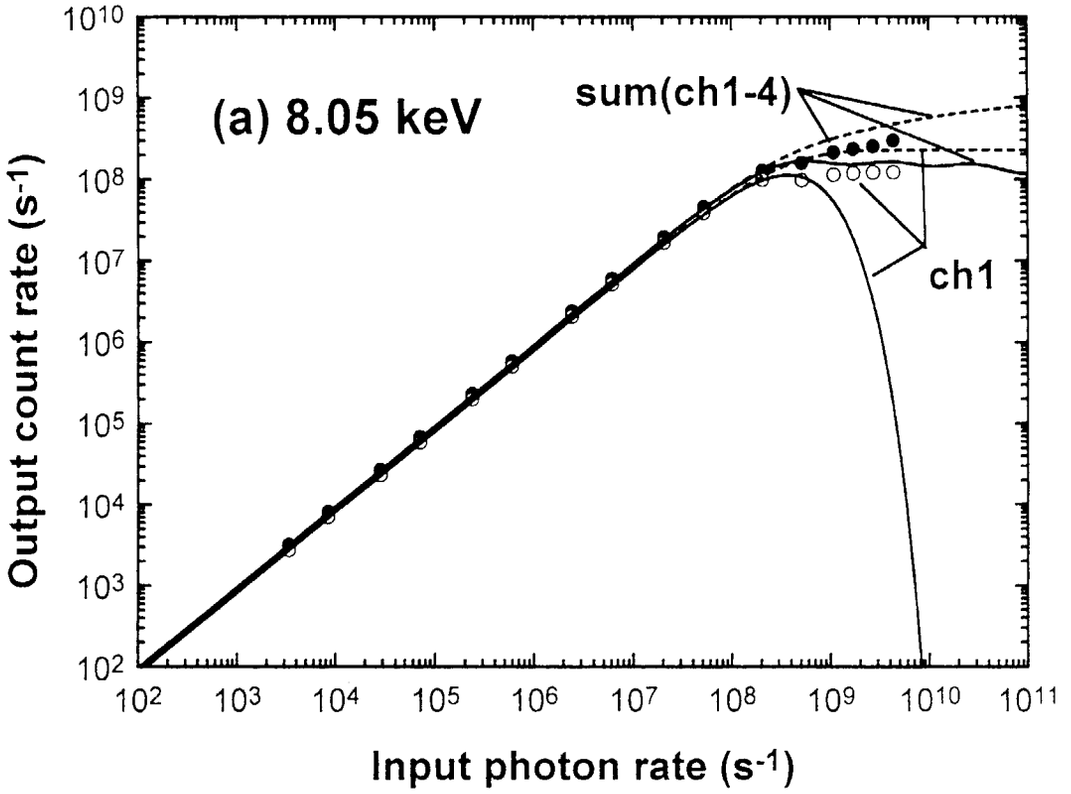
(a) 8.05 keV
sum(ch1-4)
ch1
Output count rate (s-1)
Input photon rate (s-1)
10^10
10^9
10^8
10^7
10^6
10^5
10^4
10^3
10^2
10^2
10^3
10^4
10^5
10^6
10^7
10^8
10^9
10^10
10^11

Fig.8(a)

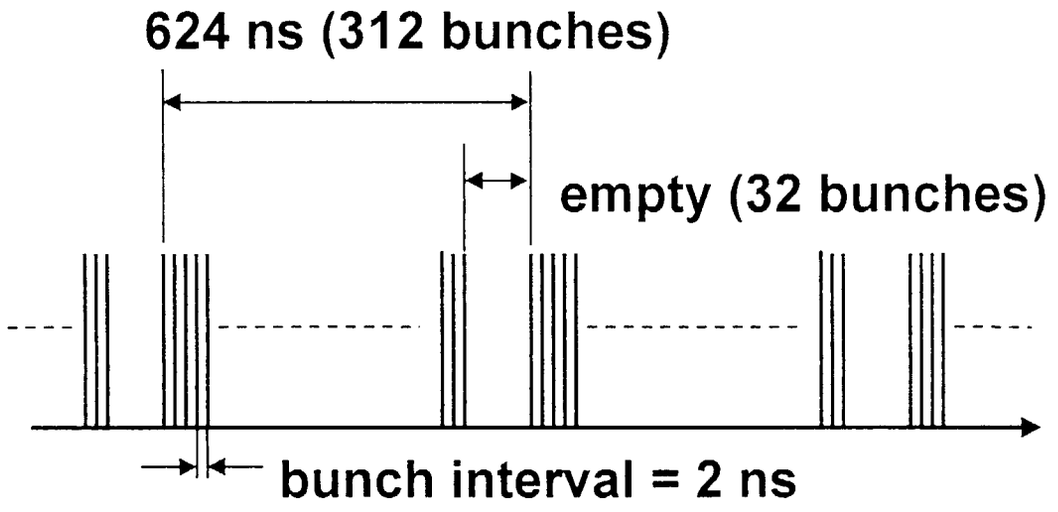
624 ns (312 bunches)
empty (32 bunches)
bunch interval = 2 ns

Fig. 7

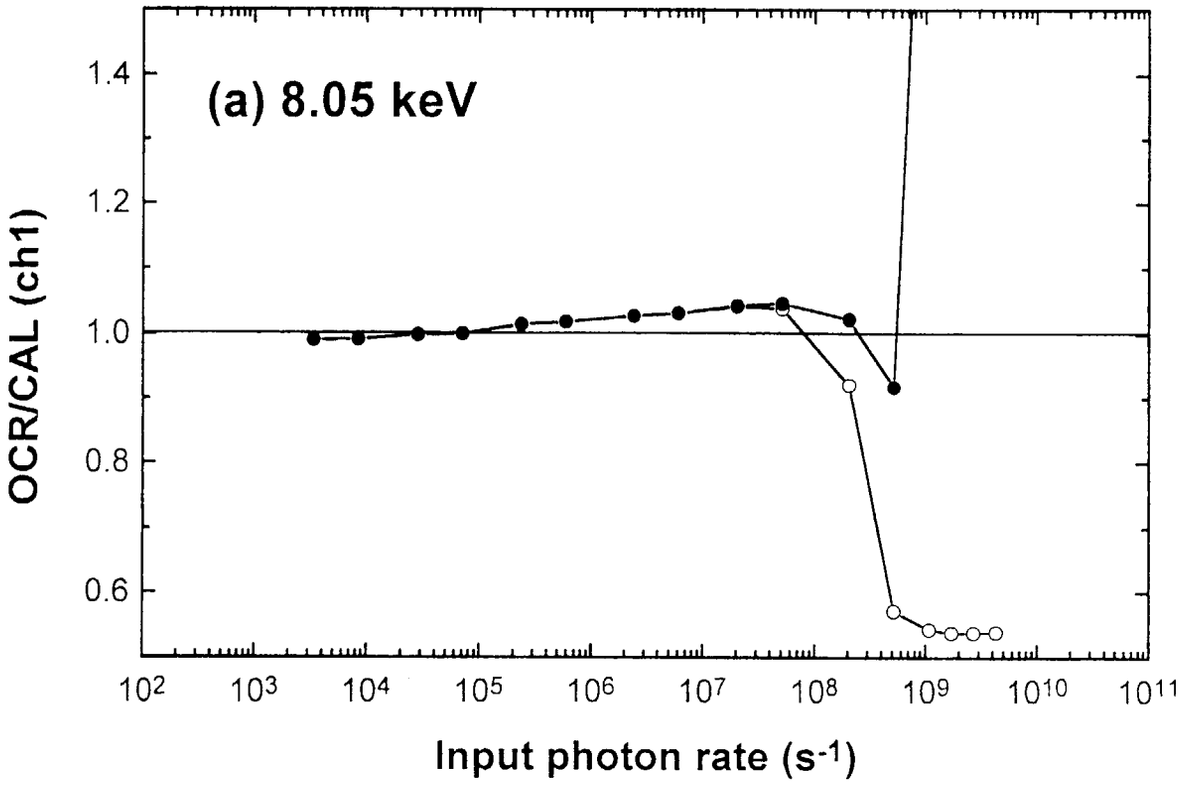
(a) 8.05 keV
OCR/CAL (ch1)
1.4
1.2
1.0
0.8
0.6
10^2 10^3 10^4 10^5 10^6 10^7 10^8 10^9 10^{10} 10^{11}
Input photon rate (s^{-1})

Fig. 9(a)

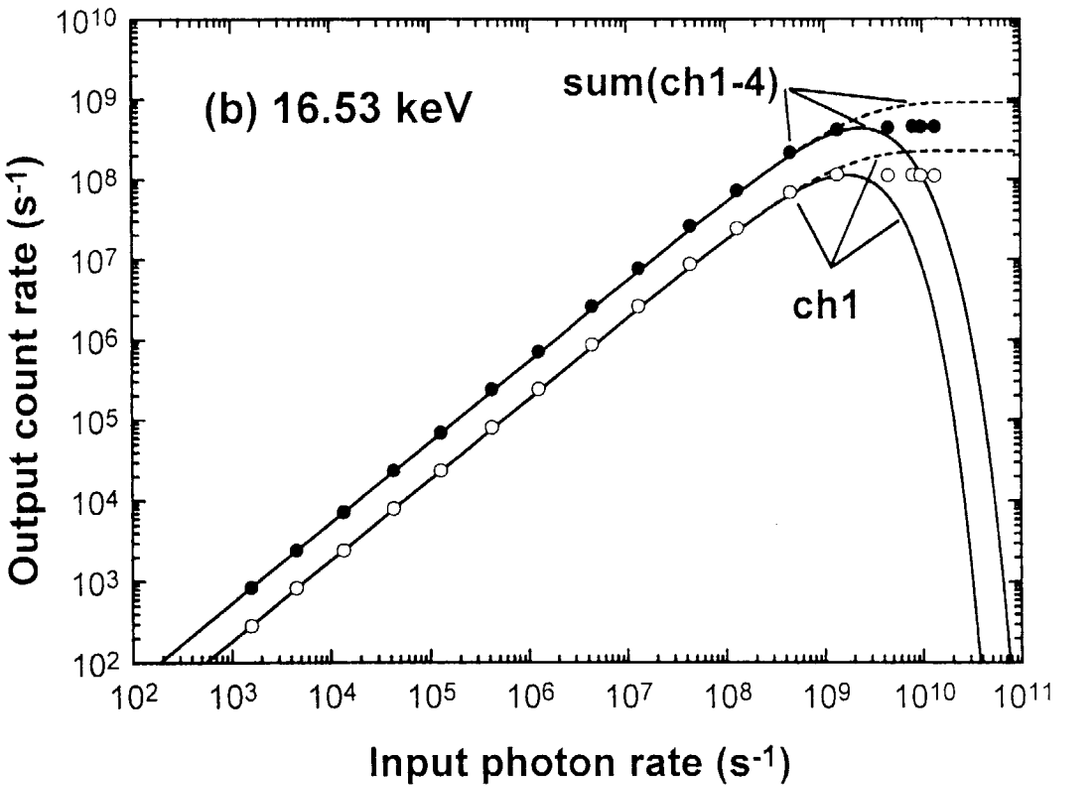
(b) 16.53 keV
sum(ch1-4)
ch1
Output count rate (s^{-1})
10^{10}
10^9
10^8
10^7
10^6
10^5
10^4
10^3
10^2
10^2 10^3 10^4 10^5 10^6 10^7 10^8 10^9 10^{10} 10^{11}
Input photon rate (s^{-1})

Fig. 8(b)

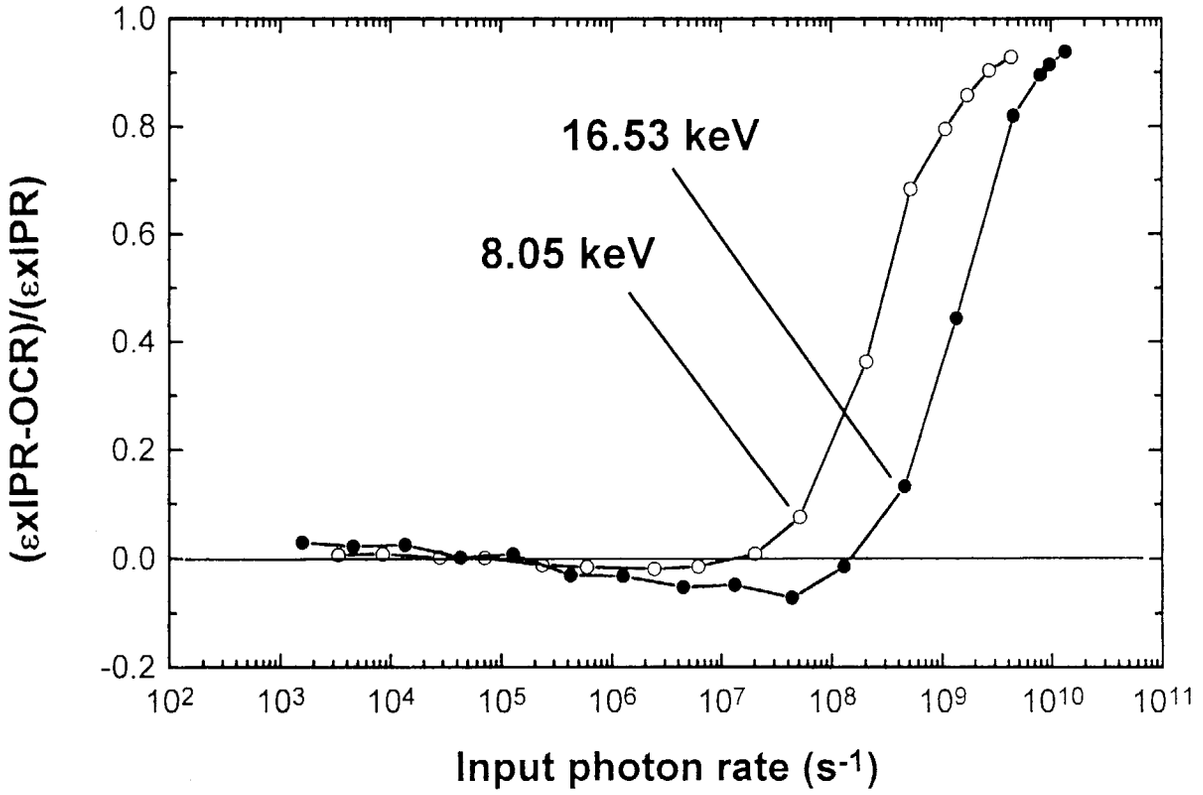
16.53 keV
8.05 keV
(εxIPR-OCR)/(εxIPR)
Input photon rate (s-1)

Fig. 10

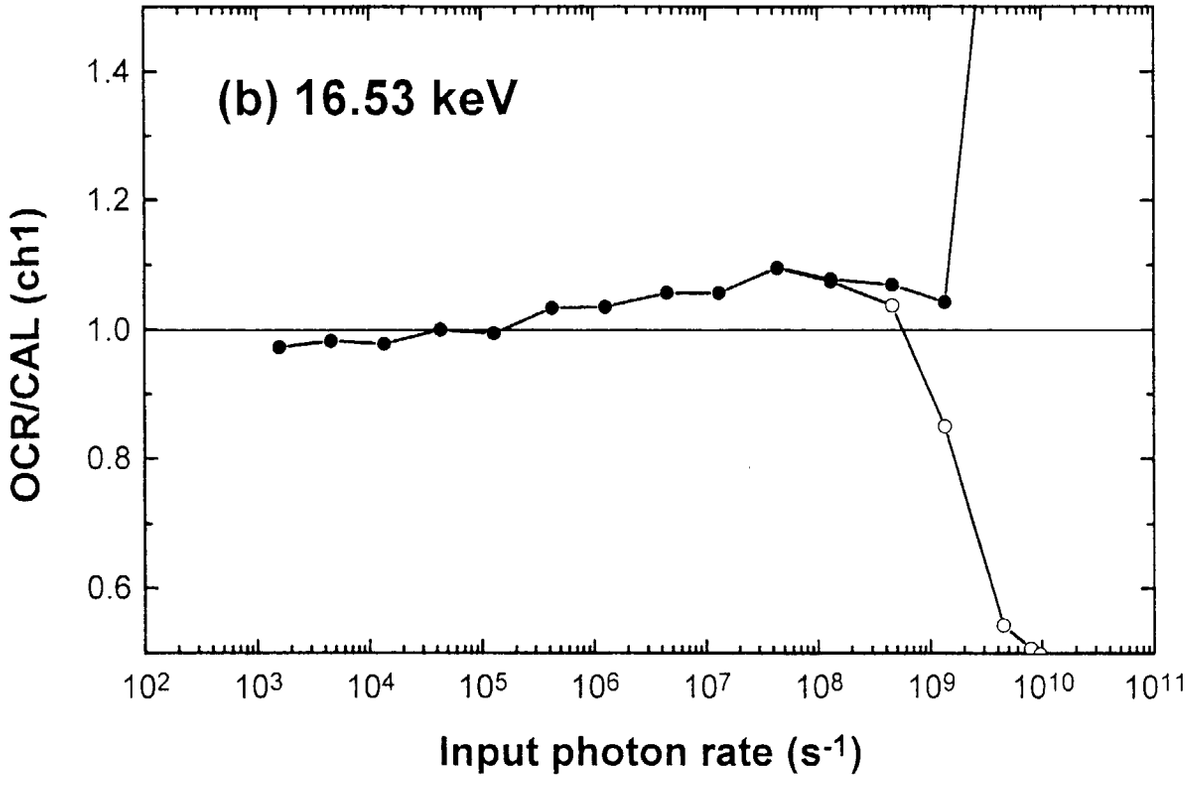
(b) 16.53 keV
OCR/CAL (ch1)
Input photon rate (s-1)

Fig. 9(b)

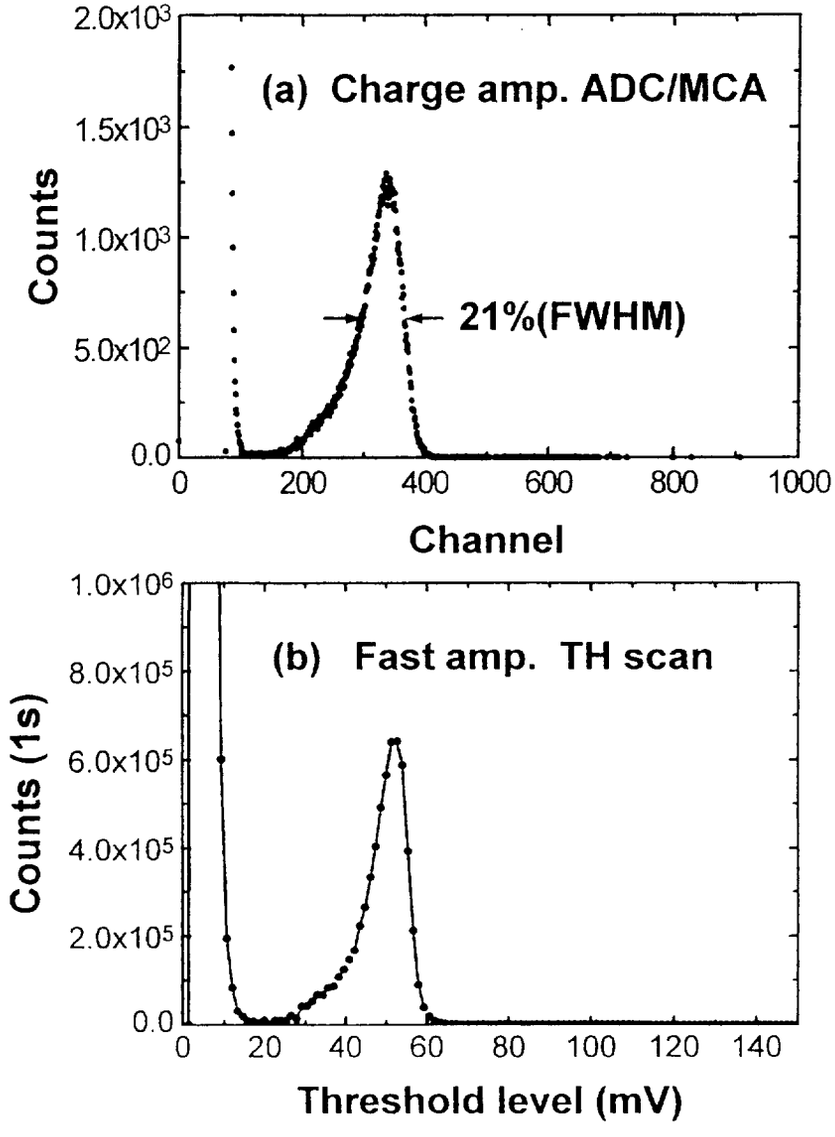
(a) Charge amp. ADC/MCA
21%(FWHM)
Counts
Channel
(b) Fast amp. TH scan
Counts (1s)
Threshold level (mV)

Fig. 11

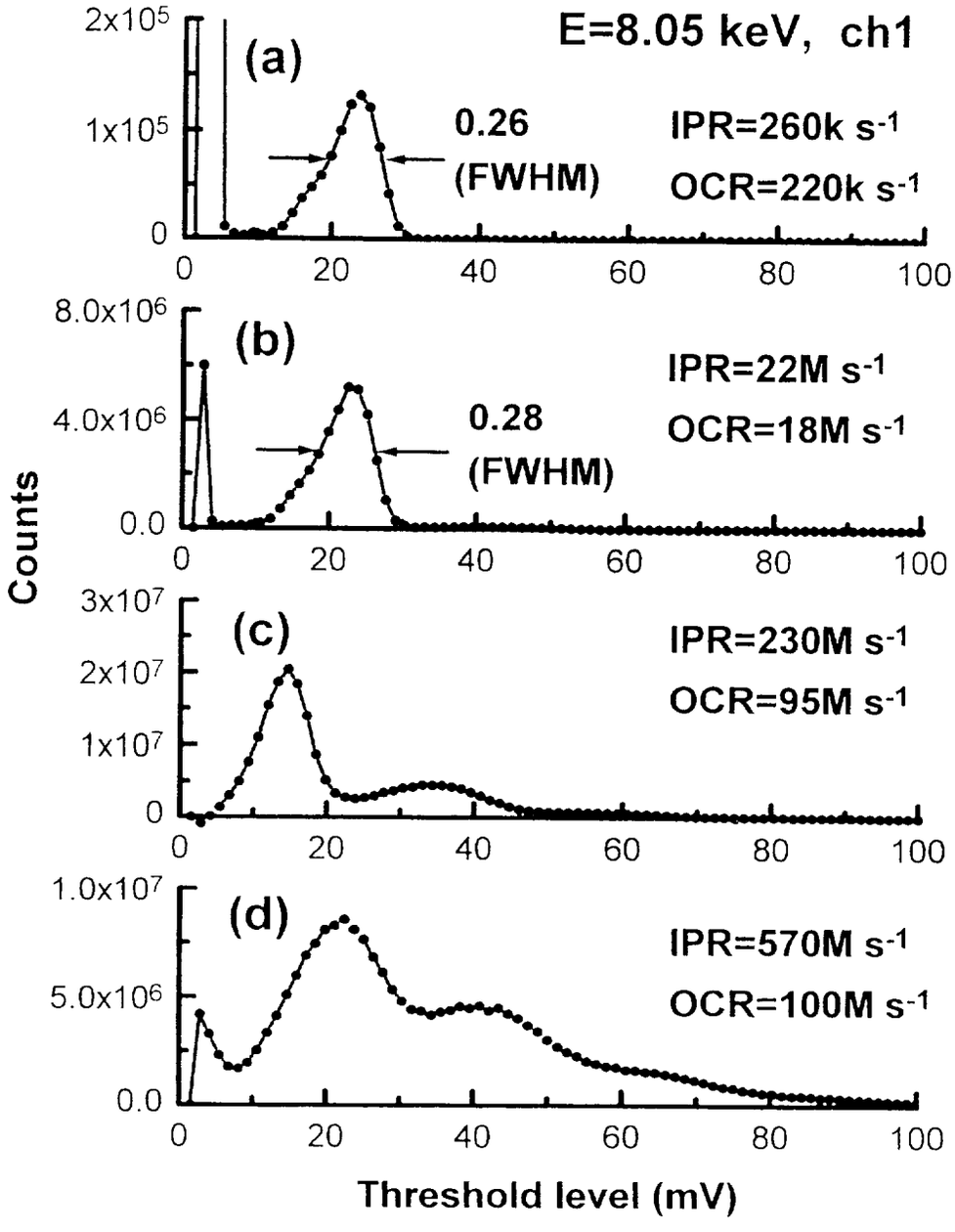
E=8.05 keV, ch1
(a)
0.26
(FWHM)
IPR=260k s-1
OCR=220k s-1
(b)
0.28
(FWHM)
IPR=22M s-1
OCR=18M s-1
(c)
IPR=230M s-1
OCR=95M s-1
(d)
IPR=570M s-1
OCR=100M s-1
Counts
Threshold level (mV)

Fig. 12